Composite Structures 160 (2017) 118–127

Contents lists available at ScienceDirect

Composite Structures

journal homepage: www.elsevier.com/locate/compstruct

Prediction of delamination of steel-polymer composites using cohesive zone model and peeling tests

Jinhyeok Jang [1], Minchang Sung [1], Sungjin Han, Woong-Ryeol Yu *

Department of Materials Science and Engineering (MSE) and Research Institute of Advanced Materials (RIAM), Seoul National University, 599 Gwanangno, Gwanak-gu, Seoul 151-742, Republic of Korea

ARTICLE INFO

Article history:
Received 9 June 2016
Revised 20 September 2016
Accepted 10 October 2016
Available online 14 October 2016

Keywords:
Sandwich structures
Delamination
Cohesive zone modeling
Peeling test

ABSTRACT

This study reports on the prediction of the delamination of steel-polymer composites. To characterize the adhesive properties from peeling tests, a simple model was derived based on peeling mechanics, in particular considering plastically dissipated energy of polymer film due to bending. Peeling tests were performed at two angles so that the adhesive properties were determined in both normal and tangential directions. Then, peel strength at arbitrary angle was predicted and compared with experiments, showing that the peel strength at only two angles and peeling mechanics considering the bending of polymer film can accurately describe the adhesive properties of steel-polymer interface. Finally, finite element simulations based on the cohesive zone model were performed to predict the delamination between steel-polymer sandwich composites, demonstrating the validity of cohesive zone model equipped with necessary properties determined using peeling tests and the developed model in this study.

1. Introduction

Steel is a core material in almost every manufacturing field due to its excellent mechanical properties. In the automotive field, steel is very widely used and much related research has been carried out. On the other hand, steel has a low damping ratio, resulting in poor noise and vibration shielding. One of the solutions to this problem is to combine steel with a polymer with a high damping property. The development of steel-polymer sandwich structures with enhanced damping properties has been the subject of much research [1,2]. The interface between the steel and the polymer has to be guaranteed for the composite to have the desired effect [3]. Generally, adhesion between the metal and the polymer is not strong, so in industrial applications, the reliability of the materials remains problematic. Accordingly, much research has focused on enhancing the interfacial properties [4,5], but the reliability of the composites, which we would like to use as structural materials, is still not guaranteed.

As the interfacial properties are important, several studies have been conducted on the characterization of delamination failures in steel-polymer sandwich composites. One method used in these studies is the virtual crack closure technique (VCCT) [6–10]. The VCCT is based on linear elastic fracture mechanics (LEFM) and the assumption that the energy release rate when an interface separates is the same as the energy required to close the crack. However, the drawback of this method is that it can only be used when there is an initial inter laminar crack in the interface. Also, it is difficult to simulate the mixed mode and progressive delamination [11–13]. Another method is cohesive zone modeling, which is based on damage mechanics. This model was first suggested by Dugdale [14], who introduced the concept, while Barenblatt [15] introduced cohesive forces on a molecular scale. Subsequently, many researchers have worked on this model for solving the delamination problem [13,16–24]. The advantage of this method is that it allows prediction of the delamination of complex structures [25,26]. Moreover, this method is simple [12] and can be easily implemented using finite element methods [17,27–29]. Therefore, cohesive zone modeling is widely used for analyzing the delamination failure in composites.

Precise methods to evaluate the interfacial properties are required for exact analysis of the delamination. These properties include the adhesion strength in both the normal and tangential directions. The most widely used method is a lap shear test [30], which measures the interfacial shear strength between the adhesive and the material in the tangential direction. Tensile adhesive

* Corresponding author.
E-mail address: woongryu@snu.ac.kr (W.-R. Yu).
[1] These authors contributed equally to this work.

http://dx.doi.org/10.1016/j.compstruct.2016.10.025
0263-8223/

Table 1
Types of surface treatments and major components on the steel surface.

Types of surface treatments	Abbreviations	Major components on surface (%)
Electro-galvanized steel	EG	Zn (87.2), C (7.67), Fe (3.1), O (1.6)
Phosphate treated steel	PL	Zn (49.8), O (23.3), C (16.5), P (5.5), Fe (1.8)
Hot dip-galvanized steel	GI	Zn (94.2), C (3.4), Fe (1.2), O (0.8)
Alloy-plated steel	GA	Zn (74.0), C (11.4), Fe (9.6), O (3.4), Al (0.8)
Mg alloy-coated steel	POSMAC	Zn (83.2), C (5.1), Al (4.3), Mg (3.1), O (2.9)

tests can be used to determine the strength in the normal direction [31]. To measure the adhesive properties when external loads are applied from various directions, corresponding test must proceed individually. In this study, we used a peeling test to measure the adhesive properties between steel and polymers, as the test is easily carried out at different angles in the same machine. Using the peel mechanics and the hypothesized plastic deformation, a simple model was derived to define the interfacial properties based on adhesive properties between the steel and polymers, which were measured from the peeling test. Finally, numerical simulations using the cohesive zone model were performed to validate our analysis.

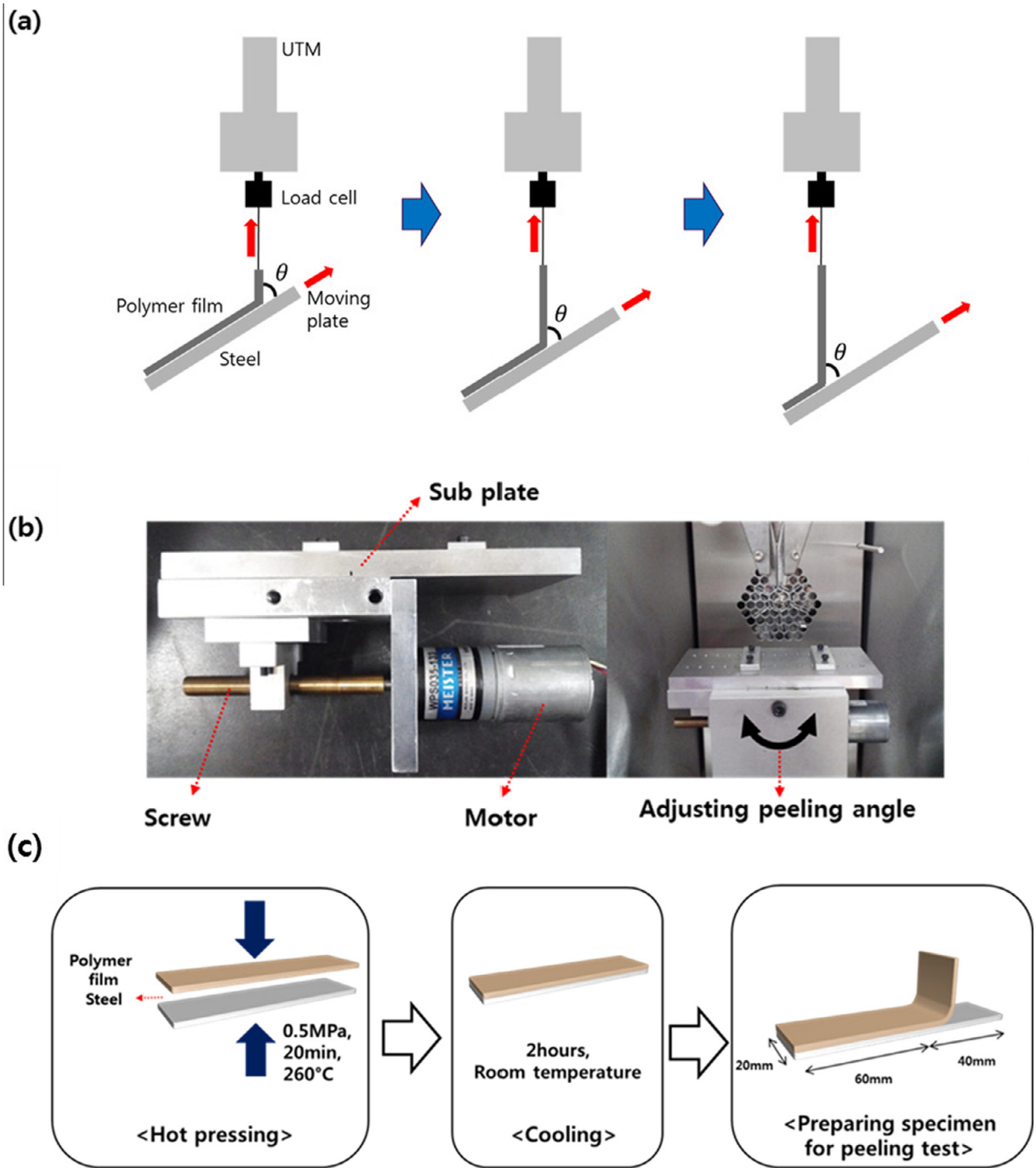

Fig. 1. (a) A schematic diagram of the apparatus used in the peeling tests, (b) the peeling apparatus built in laboratory, and (c) the method for preparing the specimens used in the peeling tests.

2. Experimental: materials and peeling test

Five types of steel were used and their surface treatment and chemical composition are summarized in Table 1. Degreased steels were supplied with different chemical compositions on their surfaces and used without any additional treatment. The polymer used in this study was nylon-6 purchased from a company (Goodfellow, UK).

Two important factors were considered when designing the apparatus for the peeling test. The first was to make a rotating sub plate which fixed the specimens. The peeling angle could be altered by rotating the sub plate. A schematic diagram of the apparatus used for the peeling test is shown in Fig. 1(a). The second factor to consider was synchronizing the origin of the peeling site. Without this synchronization, as film was peeled from the steel substrate, the peeling spot would not be fixed at the origin, meaning that the peeling angle between the pulled polymer film and the steel could not be maintained. To maintain the peeling angle, the sub plate was pulled upward by a screw attached to an electric motor (see Fig. 1(b)).

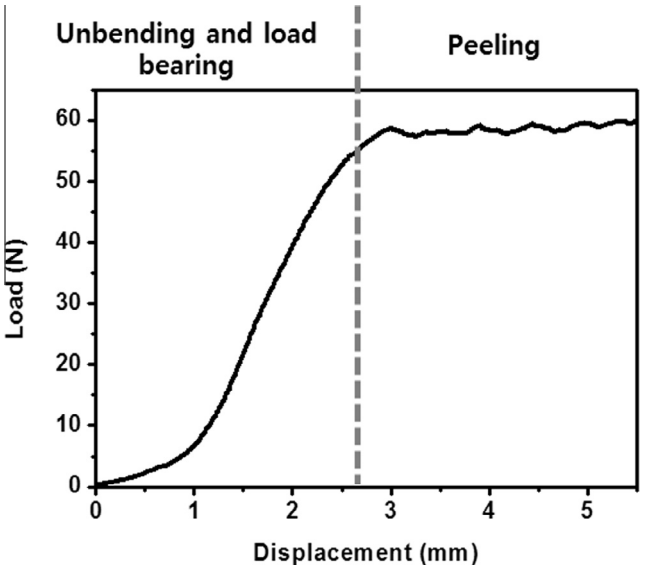

Fig. 2. Typical load-displacement curve obtained by the peeling test, showing the two stages indicated on it.

The shape and size of the specimen are shown in Fig. 1(c). Processing conditions including time, temperature, and pressure should be the same to all the specimens because adhesion properties can be affected by these conditions. After stacking nylon-6 film on the steel, a pressure of 0.5 MPa was applied using a hot press at a temperature of 260 °C. After 20 min, the sample was ejected from the hot press and cooled at room temperature for 2 h. A specific length (40 mm) of film was peeled manually to create a site that could be connected to a universal testing machine (UTM; Galdabini, Milan, Italy). The rate of peeling and the sliding speed were 5 mm/min.

In the load-displacement curve shown in Fig. 2, there was the first stage where peeling of film was not observed. In this stage, the film was tightly spread and started to bear the load. Once the peeling occurred, the second stage commenced, maintaining constant load as the peeling proceeded. The peel strength was calculated by dividing the average load during this second stage by the width of the specimen (20 mm).

3. Theoretical background

3.1. Peeling mechanics

The mechanical deformation during the peeling test was analyzed to determine the fracture energy (mode I and II) of the interface between steel and polymer, which will be used to simulate the delamination behavior via cohesive zone element. A schematic diagram of the thin film peeling from the substrate is shown in Fig. 3. The length (dL) is peeled from the substrate by force (F). In terms of geometry, b and d are the width and thickness of thin film, respectively. θ and l are, respectively, the peel angle and bending length. By conserving the energy of the peeling film through the length (dL), we know that the work done by the force is equal to the change of the energy of the system.

$$dW_p = dU_E + dU_S + dU_P + dU_K \tag{1}$$

dW_p is the work done by force, dU_E is the elastic energy in the film, dU_S is the surface energy due to the creation of new surface, dU_P is the plastically dissipated energy as the plastic bends, and dU_K is the kinetic energy. dW_p, dU_E and dU_S were derived by Kendall [32].

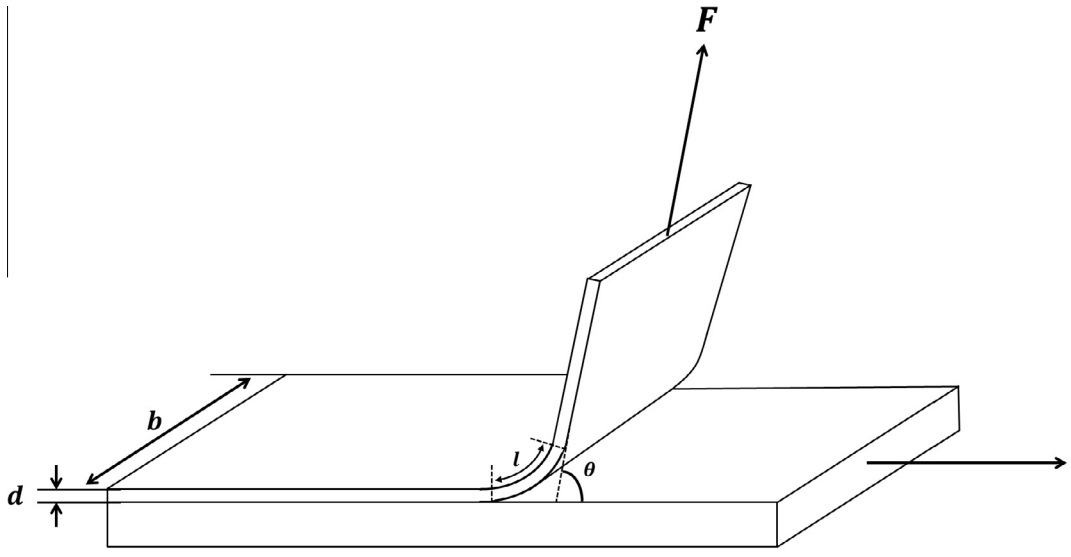

Fig. 3. Schematic illustrations of the thin film as it is peeled from the substrate.

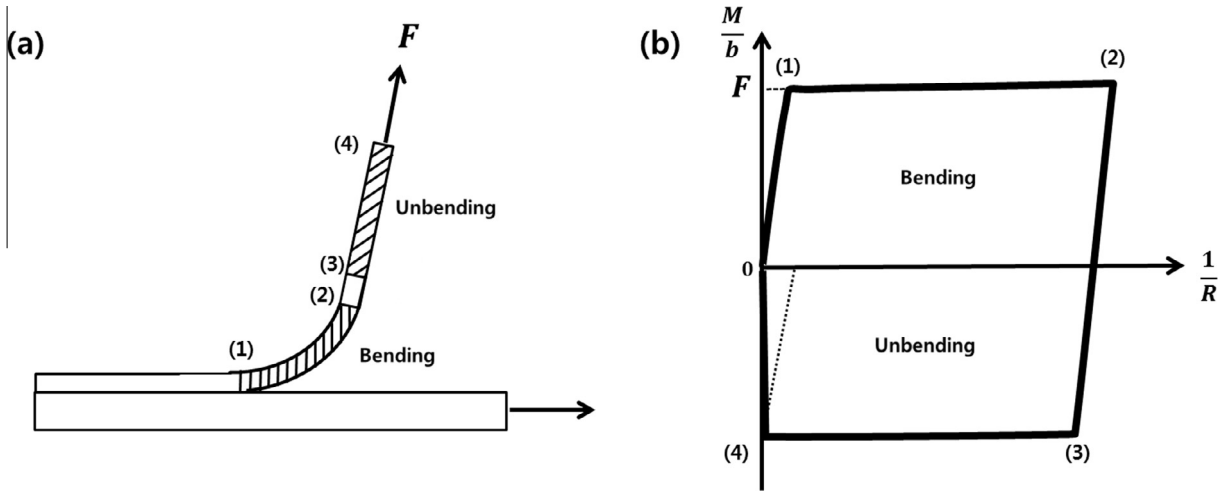

Fig. 4. (a) Schematic diagram of the plastically dissipated zone and (b) the moments of the thin film during peeling [33].

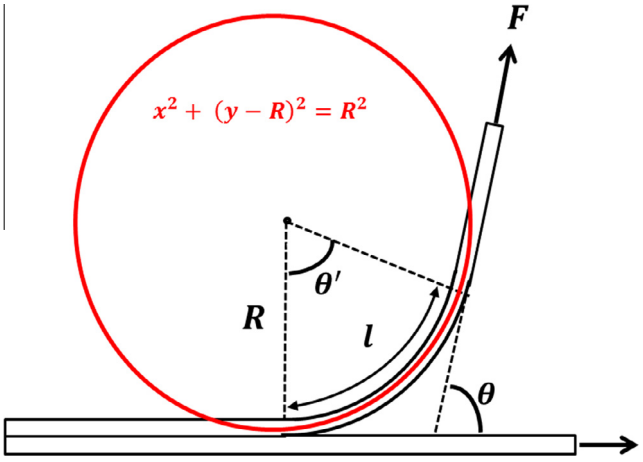

Fig. 5. Schematic illustration of the peeling thin film, assuming the uniform bending of the bending section (l).

Table 2
The bending length (l) of the samples.

Sample	l (bending length)
EG steel–nylon	4 mm
PL steel–nylon	5 mm
GI steel–nylon	24 mm
GA steel–nylon	25 mm
POSMAC steel–nylon	5 mm

$$dW_p = F(1-\cos\theta)dL + \frac{F^2}{Ebd}dL \tag{2}$$

$$dU_E = \frac{F^2}{2Ebd}dL \tag{3}$$

$$dU_s = bGdL \tag{4}$$

G is the fracture energy (adhesion energy), defined as the energy required per unit area of interface between film and substrate.

Unlike normal peeling test of thin film, polymer films behave plastically during bending because of their large thickness and adhesion between nylon and steel. To consider the influence of bending, a simplified model based on the work of Georgiou et al. [33] was derived in this study. In Fig. 4, we show plastically dissipated zone as bending and unbending occurs during the peeling process with a schematic diagram of the bending moment per unit width (M/b) and the inverse of the local radius ($1/R$). If thin film materials show no work hardening, the bending moment per unit width can be derived from the solid mechanics and beam theory:

$$\frac{M_p}{b} = \frac{\sigma_y d^2}{4} \tag{5}$$

M_p is the moment at plastic limit and σ_y is the yield strength of thin film. The total area under the curve is the plastically dissipated energy per unit width by bending. Therefore, when length (dL) is peeled from the substrate by the force (F), the plastically dissipated energy (dU_p) per unit width can be approximated.

$$dU_p \approx 2 \times \left(\frac{M_p}{b}\right) \times \left(\frac{1}{R}\right) dL \tag{6}$$

Combining Eqs. (5) and (6), the plastically dissipated energy per unit width, dU_p is derived:

$$dU_p = \left(\frac{\sigma_y d^2}{2}\right) \times \left(\frac{1}{R}\right) dL \tag{7}$$

To determine the radius of curvature (R), we assumed the uniform bending of the bending section as shown in Fig. 5. In Fig. 5, the curvature is calculated using the following:

$$R = \frac{l}{\theta'} \tag{8}$$

Based on the variation of the parameters in Fig. 5, we determined that the center angle (θ') is equal to peel angle (θ).

Table 3
Parameters of peeling nylon film from steel substrate.

ρ(density)	d (thickness)	b (width)	v (peel velocity)	θ (peel angle)
1.15 g/cm^3	0.15 mm	20 mm	5 mm/min	90°

$$\frac{dy}{dx} = \frac{R\sin\theta'}{R\cos\theta'} = \tan\theta' = \tan\theta \tag{9}$$

Finally, combining Eqs. (7), (9), the plastically dissipated energy (dU_p) per unit width is:

$$dU_p = \left(\frac{\sigma_y d^2}{2}\right) \times \left(\frac{\theta}{l}\right) dL = \left(\frac{\sigma_y d^2 \theta}{2l}\right) dL \tag{10}$$

dU_P considering the film width, b, can be written:

$$dU_p = \frac{\sigma_y b d^2 \theta}{2l} dL \tag{11}$$

To calculate the plastically dissipated energy (dU_p), the bending length (l) must be provided. We observed it from the peeling experiments. The bending length (l) was determined by averaging the measurements carried out for three different angles (60°, 90° and 120°). Note that the bending length of the nylon film from steel substrate is given in Table 2.

When the film of length (dL) is peeled from the substrate with peel velocity (v) and angle (θ), the kinetic energy (dU_K) is given by the equation below [34].

$$dU_k = \rho d b v^2 (1 - \cos\theta) dL \tag{12}$$

ρ and v are the density of film and peeling velocity, respectively. To calculate the kinetic energy, the values from Table 3 were used. The kinetic energy per unit length (dL) for all tests and samples was 2.99×10^{-8} N/mm^2, which was negligible compared to other types of energy. By combining Eqs. (1) through (4) and (11), we obtained Eq. (13).

$$F(1 - \cos\theta) dL + \frac{F^2}{Ebd} dL = \frac{F^2}{2Ebd} dL + bGdL + \frac{\sigma_y b d^2 \theta}{2l} dL \tag{13}$$

Solving for G from Eq. (13) by dividing dL and b, the fracture energy is given by,

$$G = \frac{1}{2Ed}\left(\frac{F}{b}\right)^2 + \left(\frac{F}{b}\right)(1 - \cos\theta) - \frac{\sigma_y d^2 \theta}{2l} \tag{14}$$

In this study, the fracture energy was divided into normal and tangential components, i.e., mode I and II, by two assumptions. Firstly, the contribution of the energy release rate in the normal and tangential directions (G_n and G_t) can be determined by the decomposition of the peel force. Secondly, the contribution from bending was considered only in the normal direction. Finally, G_n and G_t can be expressed as follow:

$$G_n = \frac{1}{2Ed}\left(\frac{F\sin\theta}{b}\right)^2 + \left(\frac{F\sin\theta}{b}\right)(1 - \cos\theta) - \frac{\sigma_y d^2 \theta}{2l} \tag{15}$$

$$G_t = \frac{1}{2Ed}\left(\frac{F\cos\theta}{b}\right)^2 + \left(\frac{F\cos\theta}{b}\right)(1 - \cos\theta) \tag{16}$$

The critical fracture energy of normal and tangential directions ($G_{n,c}$ and $G_{t,c}$) can be simply determined by substituting Eqs. (15) and (16) into Eq. (17), which is one of the failure criteria detailed in [35,36].

$$\left(\frac{G_n}{G_{n,c}}\right) + \left(\frac{G_t}{G_{t,c}}\right) = 1 \tag{17}$$

Combining Eqs. (15)–(17), the failure criterion can be expressed:

$$\frac{\frac{1}{2Ed}\left(\frac{F\sin\theta}{b}\right)^2 + \left(\frac{F\sin\theta}{b}\right)(1 - \cos\theta) - \frac{\sigma_y d^2 \theta}{2l}}{G_{n,c}} + \frac{\frac{1}{2Ed}\left(\frac{F\cos\theta}{b}\right)^2 + \left(\frac{F\cos\theta}{b}\right)(1 - \cos\theta)}{G_{t,c}} = 1 \tag{18}$$

Eq. (18) tells that the fracture energies in the normal and tangential directions ($G_{n,c}$ and $G_{t,c}$) can be determined using the peel strength experimentally measured at different peel angles

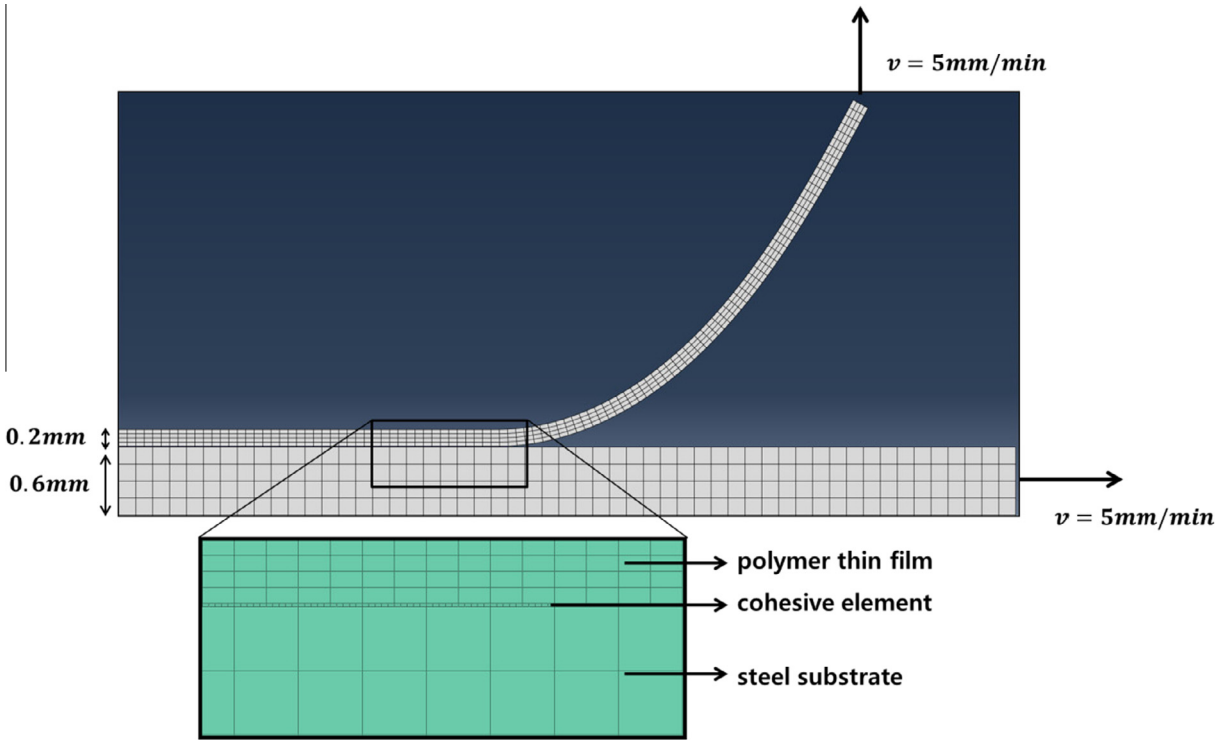

Fig. 6. Finite element model used for the simulation of the peeling test.

(in fact two different angles). From the fracture energy obtained using Eq. (18), a traction-separation law for the cohesive element can be defined, which was used to simulate the peeling experiments in this study.

3.2. Numerical model

To simulate the peel test, commercial finite element analysis software (e ABAQUS/standard, Simulia Inc., USA) was used. Following the actual experiments, a two-dimensional model was built. The geometry and boundary conditions of the numerical model are shown in Fig. 6. The interface between the steel and the polymer was modeled by a cohesive element with a thickness of 0.05 mm. Tie constraints were used to connect the cohesive elements to the steel and polymer solid.

To describe the delamination behavior of the interface, cohesive zone model was used. The adhesive layer between the steel and the polymer was represented by cohesive elements, whose delamination behavior was characterized by a traction-separation law. Many researchers have suggested different types of traction-separation law (bilinear [27,29,37], linear-parabolic [16], exponential [38,39] and trapezoidal [40,41]). Alfano et al. [42] examined the influence of the type of the traction-separation law on the analysis of debonding problems. They used a double cantilever beam test to obtain their result and concluded that the solution was independent of the type of law. Among the proposed models, the bilinear law is the most efficient in terms of CPU time, and has been used by many researchers [43–49]. Hence, a bilinear traction-separation law was used to represent the steel/polymer interface.

The bilinear traction-separation laws of the normal and tangential separations are shown in Fig. 7. During the pre-delamination stage, the cohesive element response is governed by the following elastic traction-separation relations. If the normal and tangential components are uncoupled, the elastic traction components of the 2D model can be represented using Eq. (19).

$$\begin{pmatrix} \sigma_n \\ \sigma_t \end{pmatrix} = \begin{pmatrix} K_{nn} & 0 \\ 0 & K_{tt} \end{pmatrix} \begin{pmatrix} \delta_n \\ \delta_t \end{pmatrix} \tag{19}$$

σ and δ are the traction and separation and n and t are two directions (normal and tangential), while K is the stiffness. Under normal or tangential forces, the delamination is initiated when the inter-laminar traction reaches the maximum traction ($\sigma_{n,c}$ or $\sigma_{t,c}$). Delamination propagation is predicted when the energy release rate (G_n and G_t) reaches the critical fracture energy ($G_{n,c}$ and $G_{t,c}$). The energy release rates (G_n and G_t) are calculated using Eqs. (20) and (21).

$$G_n = \int \sigma_n d\delta_n \tag{20}$$

$$G_t = \int \sigma_t d\delta_t \tag{21}$$

The critical fracture energy ($G_{n,c}$ and $G_{t,c}$) is formulated using Eqs. (22) and (23).

Table 4
The peel strengths measured in the peeling tests.

Sample	Angle (degree)	Peel strength (N/mm)	
		Average	Standard deviation
EG steel–nylon	60	4.302	0.279
	90	2.897	0.239
	120	2.324	0.178
PL steel–nylon	60	4.079	0.346
	90	2.753	0.217
	120	2.197	0.195
GI steel–nylon	60	0.451	0.200
	90	0.415	0.109
	120	0.288	0.150
GA steel–nylon	60	1.728	0.155
	90	1.208	0.066
	120	0.969	0.025
POSMAC steel–nylon	60	3.623	0.275
	90	2.339	0.148
	120	1.892	0.179

Table 5
Fracture energies ($G_{n,c}$ and $G_{t,c}$) between the steel and nylon interface determined using experiment and Eq. (18).

Sample	$G_{n,c}$ (kJ/m^2)	$G_{t,c}$ (kJ/m^2)
EG steel–nylon	2.73	3.15
PL steel–nylon	2.58	2.83
GI steel–nylon	0.38	0.20
GA steel–nylon	1.17	1.15
POSMAC steel–nylon	2.16	2.22

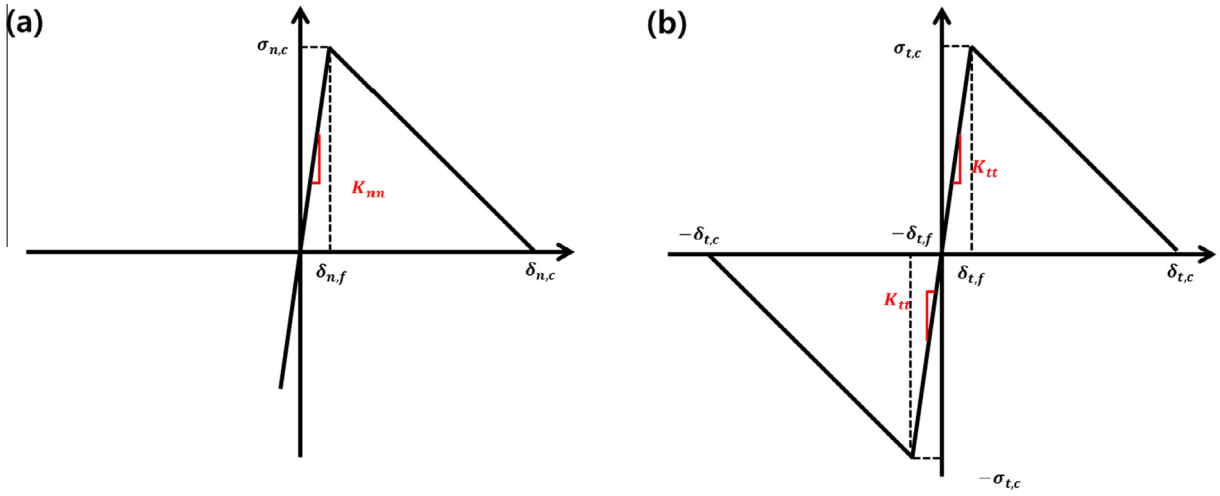

Fig. 7. Bilinear traction-separation law: (a) Normal direction. (b) Tangential direction.

$$G_{n,c} = \frac{1}{2}\sigma_{n,c}\delta_{n,c} \tag{22}$$

$$G_{t,c} = \frac{1}{2}\sigma_{t,c}\delta_{t,c} \tag{23}$$

δ_c is the critical separation length of the cohesive element. We used failure initiation and propagation criteria when considering the mixed mode loading condition. The failure initiation value inducing delamination was evaluated using the quadratic criterion (Eq. (24) below) suggested by Ye [50]. The failure propagation criterion for continued delamination was evaluated using the power law criterion (Eq. (25)) suggested by Long [51].

$$\left(\frac{\sigma_n}{\sigma_{n,c}}\right)^2 + \left(\frac{\sigma_t}{\sigma_{t,c}}\right)^2 = 1 \tag{24}$$

$$\left(\frac{G_n}{G_{n,c}}\right) + \left(\frac{G_t}{G_{t,c}}\right) = 1 \tag{25}$$

In the simulation, the critical fracture energy ($G_{n,c}$ and $G_{t,c}$) was determined by experimentally obtained peel strength (as described in Section 3.1). Alfano et al. [29] found that variations in the maximum traction did not have a significant influence on the delamination prediction. Previous studies suggested the minimum number of elements required for the cohesive zone to be successfully applied to the prediction of delamination [52,53]. To guarantee a sufficient number of elements in the cohesive zone, the maximum traction ($\sigma_{n,c}$ or $\sigma_{t,c}$) was set to be 10 MPa. The stiffness (K_{nn} and K_{tt}) was set to be 10^6 N/mm^3 following the suggestion of previous studies [24,54]. The critical separation length ($\delta_{n,c}$ $G_{n,c}$ and $\delta_{t,c}$) were calculated using Eqs. (22) and (23) with the critical fracture energy (and $G_{t,c}$) provided.

4. Results and discussion

The peel strengths at angles 60°, 90° and 120° were measured using the peeling test (see Table 4). In this study, the peeling test was repeated at least 5 times for each specimen to obtain reliable data. It is clear from Table 4 that as the peel angle decreased, the peel strength increased. This result agrees with previous studies [55–57]. The peel strength was strongly dependent on the steel surface, in particular its chemical composition. Especially, oxygen is considered as one of main factor to improve the peel strength as a result of relatively strong hydrogen bonding between steel and nylon-6. As such, high oxygen content on the surface of phosphate-treated steel (PL) formed a strong interface with the polymer, while low oxygen content of the surface of hot dip-galvanized steel (GI) brought about small peel strength and oxygen contents were small.

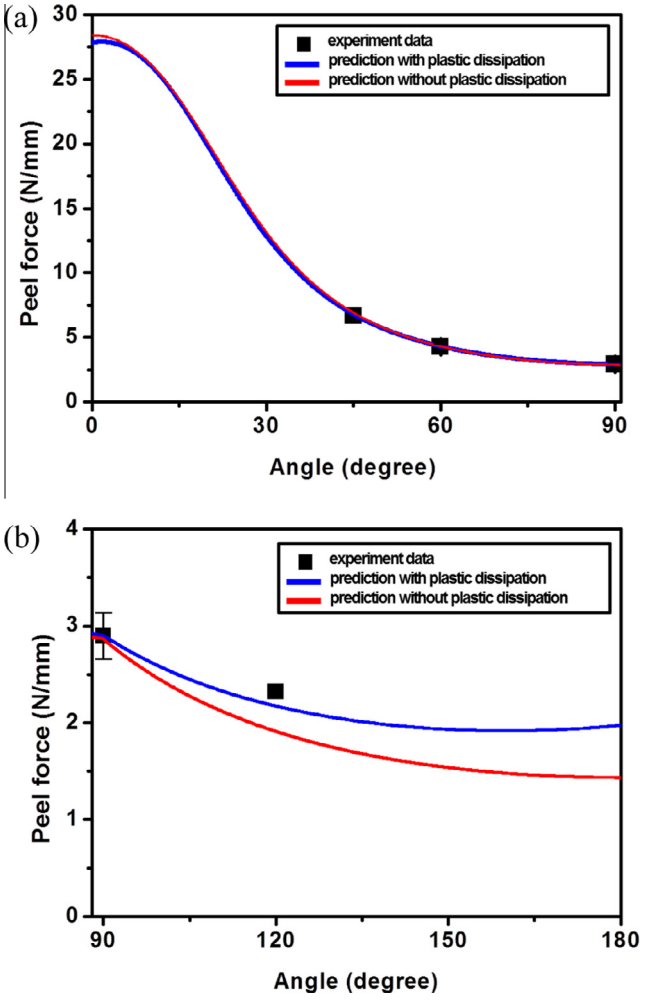

Fig. 8. Comparison of experimental and predicted peel strengths for different peel angles in the case of EG steel and nylon 6. (a) 0–90 degrees and (b) 90–180 degrees. Note that peel strength for all peeling angles were predicted using two peel strength at 60° and 90° and Eq. (18). For comparison purpose, peel strength measured at 45° and 120° were also provided.

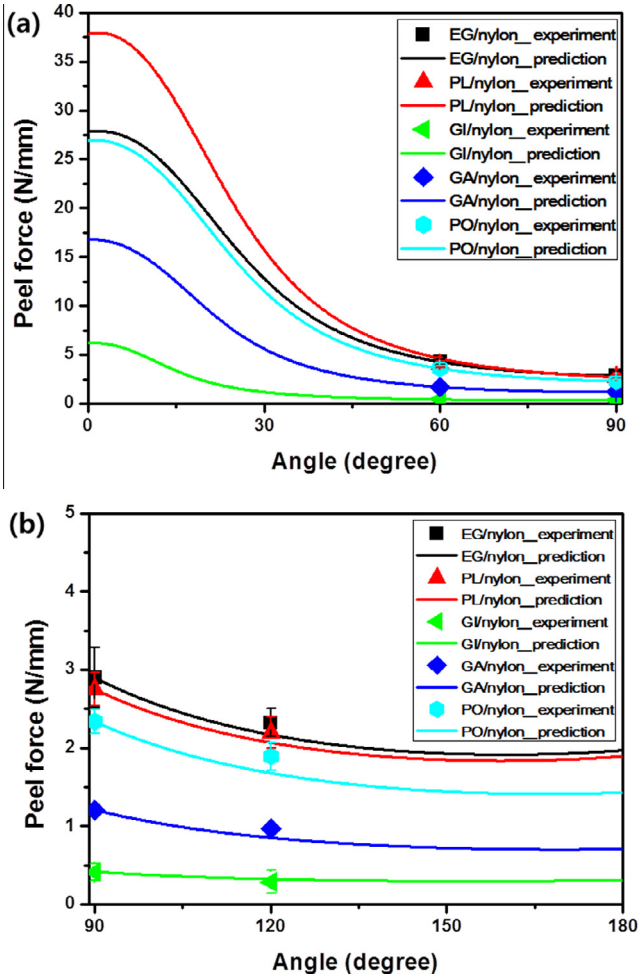

Fig. 9. Comparison of experimental and predicted peel strengths for different peel angles for different peel angles: (a) 0–90 degrees and (b) 90–180 degrees.

To define the adhesive properties between the steel and nylon, the fracture energy in both the normal and tangential directions ($G_{n,c}$ and $G_{t,c}$) were calculated using the peel strengths at 60° and 90° and Eq. (18). The data in Table 5 show that the values of and depend significantly on the substrate and on the direction. Generally, was higher than. In the case of having high adhesive properties (EG, PL, POSMAC steel–nylon), a similar trend was shown. However, in the case of having low adhesive properties (GI, GA steel–nylon), the opposite trend was shown. The reason for this is that the experimental error of peel measurement increased when the interface between layers was too weak, so causing the opposite results. These values $G_{n,c}$ and $G_{t,c}$ were used to predict the peel strength for other peel angles and set up the traction–separation laws of the cohesive elements.

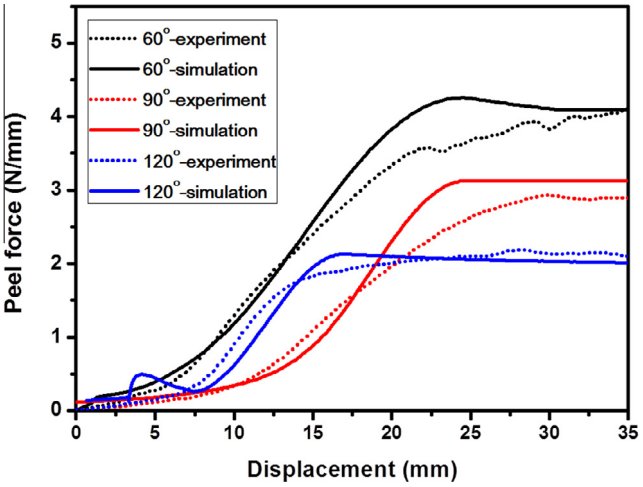

Fig. 10. Comparison of simulated peel force with experimental one according to peel displacement in case of EG steel–nylon 6.

Using the critical fracture energy ($G_{n,c}$ and $G_{t,c}$), peel strength (F/b in Eq. (18)) for all angles were predicted. In Fig. 8, the predicted peel strength between EG steel and nylon were presented and compared with peel strength measured for angles 45° and 120°, demonstrating that the peel strength at all angles can be predicted using the peel strength at only two angles and Eq. (18). In low peel angles (0–90°), there was no significant difference when bending was considered (see Fig. 8(a)). However, in high peel angle (90–180°), a significant difference between prediction and experiment was observed due to increasing influence of the bending (see Fig. 8(b)). Therefore, in the case of peeling polymer film from steel substrate, the consideration of bending is essential to predict accurate interface properties. Predicted peel strength for other substrates are compared with experimentally determined peel strength in Fig. 9, showing that there is good agreement between the theoretical prediction from Eq. (18) and the experimentally measured peel strength.

To validate our model using a cohesive zone model, whose parameters can be effectively determined by the peeling mechanics and experiments explained in Section 3, numerical analysis was carried out to simulate the peeling behavior of steel-polymer composites at 60°, 90° and 120°. We compared the experimental and simulated peel force as a function of peel displacement. The variation of the peel force with the displacement for different angles in the case of EG steel and nylon is shown in Fig. 10. Steady-state peel forces, which do not depend on the angle, were also obtained. The peel forces simulated using finite element analysis with cohesive elements agreed well with experimental results. The peel front

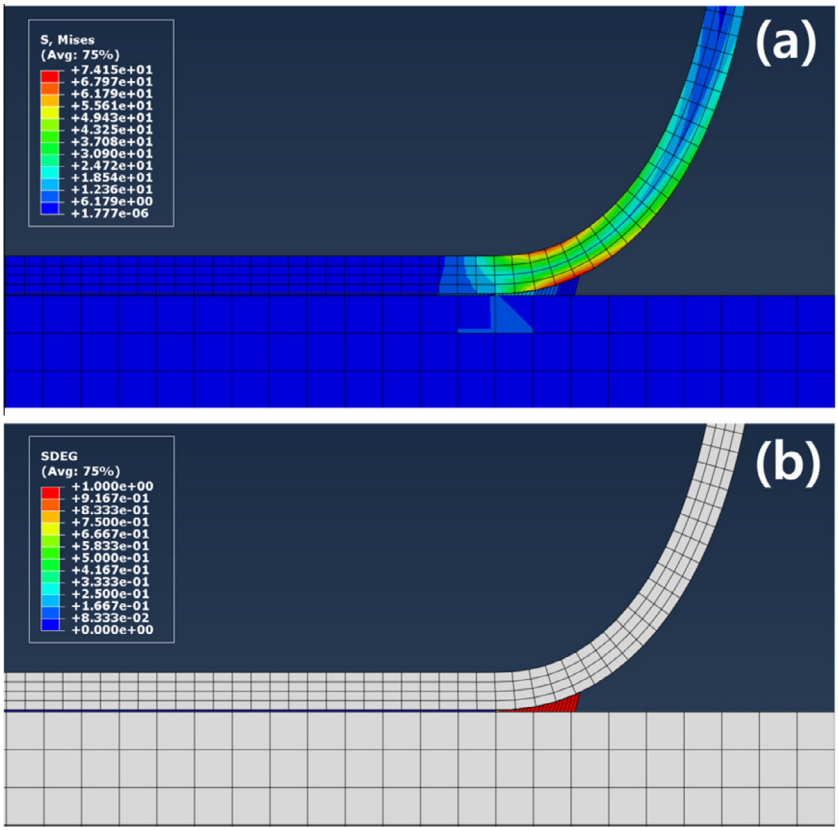

Fig 11. Simulation results showing (a) Mises stress and (b) overall scalar stiffness degradation (SDEG) in the cohesive layer during peeling.

Table 6
Comparison of the peel strength determined by finite element analysis with experimental one.

Sample	Angle (degree)	Peel strength (N/mm)		
		Experiment	Simulation	Difference (%)
EG steel–nylon	60	4.302	4.297	0.116
	90	2.897	2.943	1.588
	120	2.324	2.154	7.315
PL steel–nylon	60	4.079	4.191	2.739
	90	2.753	2.769	0.596
	120	2.197	2.211	0.648
GI steel–nylon	60	0.451	0.447	0.949
	90	0.415	0.390	5.938
	120	0.288	0.285	0.987
GA steel–nylon	60	1.728	1.689	2.243
	90	1.208	1.204	0.332
	120	0.969	0.891	8.356
POSMAC steel–nylon	60	3.623	3.499	3.395
	90	2.339	2.410	3.045
	120	1.892	1.721	9.038

and delamination zone of the peel arms are shown in Fig. 11. High stress concentrated on the peel arm because of the bending. After peeling, the part of the film far from the delamination zone did not undergo stress, as shown in Fig. 11(a), and almost no energy dissipated in the part of the film located above the delamination zone. In Fig. 11(b), the overall scalar stiffness degradation of the cohesive element during the peeling is shown. For this figure, the cohesive zone consisted of 10 cohesive elements. The cohesive elements were not degraded before the failure was initiated. After the failure initiation, as determined by the failure initiation criterion, the degradation started. Finally, after the peeling satisfied the propagation criterion of failure, the cohesive elements did not undergo further traction. The experimental and simulated peel strengths are compared in Table 6. The results indicate that it is possible to simulate the peel behavior to an accuracy of 10% in all cases using cohesive zone models. Therefore, it can be concluded that the proposed method used to evaluate the adhesive properties, which was based on peeling tests and our derived failure criterion (Eq. (18)), was appropriate for modeling the steel-polymer interface.

5. Conclusion

Peeling tests were performed to measure the adhesive properties between steel and polymer (nylon). A theoretical approach was also developed to identify the adhesive properties between steel and nylon. Based on the peeling mechanics and consideration of plastically dissipated energy by bending, a simple model was derived to characterize the adhesive properties in both the normal and tangential directions. Two example calculation were provided to validate the current approach. First, the peel strength between steel and polymer at an arbitrary angle was predicted and compared with experiments, demonstrating that the consideration of the bending of polymer film during peeling is essential to improving the prediction accuracy. Next, finite element simulation of peeling process was carried out using a cohesive zone model. It was concluded that the failures due to delamination in steel-polymer sandwich composites can be predicted using the cohesive zone model equipped with necessary properties determined using peeling tests and the simple model developed in this study.

Acknowledgement

This work was supported by the National Research Foundation of Korea (NRF) grant funded by the Ministry of Science, ICT & Future Planning (MSIP) (NO. NRF-2015R1A5A1037627) and the Research center for Strategic materials by POSCO (No. 2014Z066).

References

[1] Nakra B. Vibration control in machines and structures using viscoelastic damping, 1998.
[2] Kari L et al. Constrained polymer layers to reduce noise: reality or fiction?—an experimental inquiry into their effectiveness. Polym Test 2002;21(8):949–58.
[3] Matsumoto Y et al. Effect of the adhesive strength on the bendability of vibration-damping composite steel sheet. Trans Iron Steel Inst Jpn 1986;26 (10):903–5.
[4] Venables J. Adhesion and durability of metal-polymer bonds. J Mater Sci 1984;19(8):2431–53.
[5] Mathieson I, Bradley R. Improved adhesion to polymers by UV/ozone surface oxidation. Int J Adhes Adhes 1996;16(1):29–31.
[6] Robinson P, Javidrad F, Hitchings D. Finite element modelling of delamination growth in the DCB and edge delaminated DCB specimens. Compos Struct 1995;32(1):275–85.
[7] Irwin GR. Analysis of stresses and strains near the end of a crack traversing a plate. SPIE milestone series MS. J Appl Mech 1997;137:167–70.
[8] Rybicki EF, Kanninen M. A finite element calculation of stress intensity factors by a modified crack closure integral. Eng Fract Mech 1977;9(4):931–8.
[9] Shokrieh M et al. Simulation of mode I delamination propagation in multidirectional composites with R-curve effects using VCCT method. Comput Mater Sci 2012;65:66–73.
[10] Pereira A, De Morais A. Mode I interlaminar fracture of carbon/epoxy multidirectional laminates. Compos Sci Technol 2004;64(13):2261–70.
[11] Alfano G, Sacco E. Combining interface damage and friction in a cohesive-zone model. Int J Numer Meth Eng 2006;68(5):542–82.
[12] Turon A et al. A damage model for the simulation of delamination in advanced composites under variable-mode loading. Mech Mater 2006;38(11):1072–89.
[13] Turon A et al. An engineering solution for mesh size effects in the simulation of delamination using cohesive zone models. Eng Fract Mech 2007;74 (10):1665–82.
[14] Dugdale D. Yielding of steel sheets containing slits. J Mech Phys Solids 1960;8 (2):100–4.
[15] Barenblatt GI. The mathematical theory of equilibrium cracks in brittle fracture. Adv Appl Mech 1962;7(1):55–129.
[16] Allix O, Ladeveze P, Corigliano A. Damage analysis of interlaminar fracture specimens. Compos Struct 1995;31(1):61–74.
[17] Schellekens J, De Borst R. A non-linear finite element approach for the analysis of mode-I free edge delamination in composites. Int J Solids Struct 1993;30 (9):1239–53.
[18] Bažant Z, Grassl P. Size effect of cohesive delamination fracture triggered by sandwich skin wrinkling. J Appl Mech 2007;74(6):1134–41.
[19] Harper PW, Hallett SR. Cohesive zone length in numerical simulations of composite delamination. Eng Fract Mech 2008;75(16):4774–92.
[20] Aymerich F, Dore F, Priolo P. Prediction of impact-induced delamination in cross-ply composite laminates using cohesive interface elements. Compos Sci Technol 2008;68(12):2383–90.
[21] Borg R, Nilsson L, Simonsson K. Simulation of delamination in fiber composites with a discrete cohesive failure model. Compos Sci Technol 2001;61 (5):667–77.
[22] Aymerich F, Dore F, Priolo P. Simulation of multiple delaminations in impacted cross-ply laminates using a finite element model based on cohesive interface elements. Compos Sci Technol 2009;69(11):1699–709.
[23] Borg R, Nilsson L, Simonsson K. Modeling of delamination using a discretized cohesive zone and damage formulation. Compos Sci Technol 2002;62 (10):1299–314.
[24] Camanho PP, Davila C, De Moura M. Numerical simulation of mixed-mode progressive delamination in composite materials. J Compos Mater 2003;37 (16):1415–38.

[25] Turon Travesa A. Simulation of delamination in composites under quasi-static and fatigue loading using cohesive zone models. Universitat de Girona; 2006.
[26] Andreasson E, Jemal A, Katangoori RR. Is it possible to open beverage packages virtually? Physical tests in combination with virtual tests in Abaqus. In: SIMULIA Community Conference (SCC), Simulia; 2012.
[27] Mi Y et al. Progressive delamination using interface elements. J Compos Mater 1998;32(14):1246–72.
[28] Goyal VK, Johnson ER, Davila CG. Irreversible constitutive law for modeling the delamination process using interfacial surface discontinuities. Compos Struct 2004;65(3):289–305.
[29] Alfano G, Crisfield M. Finite element interface models for the delamination analysis of laminated composites: mechanical and computational issues. Int J Numer Meth Eng 2001;50(7):1701–36.
[30] Berger EJ. A method of determining the surface acidity of polymeric and metallic materials and its application to lap shear adhesion. J Adhes Sci Technol 1990;4(1):373–91.
[31] Shimizu K et al. Improved adhesion between PMMA and stainless steel modified with PMMA brushes. ACS Appl Mater Interfaces 2014;6 (23):21308–15.
[32] Kendall K. Thin-film peeling-the elastic term. J Phys D Appl Phys 1975;8 (13):1449.
[33] Georgiou I et al. Cohesive zone models and the plastically deforming peel test. J Adhes 2003;79(3):239–65.
[34] Creton C et al. The mechanics of adhesion. Adhes Sci Eng 2002:535–76.
[35] De Lorenzis L, Zavarise G. Modeling of mixed-mode debonding in the peel test applied to superficial reinforcements. Int J Solids Struct 2008;45(20):5419–36.
[36] De Moura M et al. Cohesive and continuum mixed-mode damage models applied to the simulation of the mechanical behaviour of bonded joints. Int J Adhes Adhes 2008;28(8):419–26.
[37] Hillerborg A, Modéer M, Petersson P-E. Analysis of crack formation and crack growth in concrete by means of fracture mechanics and finite elements. Cem Concr Res 1976;6(6):773–81.
[38] Xu X-P, Needleman A. Numerical simulations of fast crack growth in brittle solids. J Mech Phys Solids 1994;42(9):1397–434.
[39] Chandra N et al. Some issues in the application of cohesive zone models for metal–ceramic interfaces. Int J Solids Struct 2002;39(10):2827–55.
[40] Tvergaard V, Hutchinson JW. On the toughness of ductile adhesive joints. J Mech Phys Solids 1996;44(5):789–800.
[41] Tvergaard V, Hutchinson JW. The influence of plasticity on mixed mode interface toughness. J Mech Phys Solids 1993;41(6):1119–35.
[42] Alfano G. On the influence of the shape of the interface law on the application of cohesive-zone models. Compos Sci Technol 2006;66(6):723–30.
[43] Turon A et al. Accurate simulation of delamination growth under mixed-mode loading using cohesive elements: definition of interlaminar strengths and elastic stiffness. Compos Struct 2010;92(8):1857–64.
[44] Ye Q, Chen P. Prediction of the cohesive strength for numerically simulating composite delamination via CZM-based FEM. Compos Part B 2011;42 (5):1076–83.
[45] De Moura M, Gonçalves J. Cohesive zone model for high-cycle fatigue of adhesively bonded joints under mode I loading. Int J Solids Struct 2014;51 (5):1123–31.
[46] Lee MJ et al. Determination of cohesive parameters for a mixed-mode cohesive zone model. Int J Adhes Adhes 2010;30(5):322–8.
[47] Arablouei A, Kodur V. Cohesive zone model properties for evaluating delamination of spray-applied fire-resistive materials from steel structures. Eng Fract Mech 2015;143:138–57.
[48] Pelfrene J, Van Dam S, Van Paepegem W. Numerical analysis of the peel test for characterisation of interfacial debonding in laminated glass. Int J Adhes Adhes 2015;62:146–53.
[49] Guo X, Su R, Young B. Numerical investigation of the bilinear softening law in the cohesive crack model for normal-strength and high-strength concrete. Adv Struct Eng 2012;15(3):373–88.
[50] Ye L. Role of matrix resin in delamination onset and growth in composite laminates. Compos Sci Technol 1988;33(4):257–77.
[51] Long R. Static strength of adhesively bonded ARALL-1 joints. J Compos Mater 1991;25(4):391–415.
[52] Moës N, Belytschko T. Extended finite element method for cohesive crack growth. Eng Fract Mech 2002;69(7):813–33.
[53] Falk ML, Needleman A, Rice JR. A critical evaluation of cohesive zone models of dynamic fracture. J Phys IV 2001;11(PR5). Pr5-43–Pr5-50.
[54] Zou Z et al. Modelling interlaminar and intralaminar damage in filament-wound pipes under quasi-static indentation. J Compos Mater 2002;36 (4):477–99.
[55] Kinloch A, Lau C, Williams J. The peeling of flexible laminates. Int J Fract 1994;66(1):45–70.
[56] Molinari A, Ravichandran G. Peeling of elastic tapes: effects of large deformations, pre-straining, and of a peel-zone model. J Adhes 2008;84 (12):961–95.
[57] Thouless MD, Jensen HM. Elastic fracture mechanics of the peel-test geometry. J Adhes 1992;38(3–4):185–97.